

201122017A

厚生労働科学研究費補助金

障害者対策総合研究事業

ポリグルタミン病の分子病態機序に基づく

分子標的治療法の開発

平成23年度 総括研究報告書

研究代表者 辻 省 次

平成24（2012）年 3月

目 次

I. 総括研究報告

ポリグルタミン病の分子病態機序に基づく分子標的治療法の開発に関する研究

辻 省 次

II. 研究成果の刊行物・別刷

厚生労働科学研究補助金(障害者対策総合研究事業)

総括研究報告書

ポリグルタミン病の分子病態機序に基づく分子標的治療法の開発

研究代表者 辻 省次 東京大学医学部附属病院 神経内科教授

研究要旨:本研究では、歯状核赤核淡蒼球ルイ体萎縮症(DRPLA)の治療法開発を目指して、病因遺伝子の産物である DRPLA protein の生理的機能を解明し、その知見に基づき分子病態機序明らかにし、その上で、有効な治療法の対象となる分子標的を定め、分子標的治療法を実現することを目的としている。これまでの研究で、DRPLA protein の核内局在を阻害、あるいは、核内での局在パターンを変させる物質として 34 種類の化合物を見出した。その中の1つについて、DRPLA モデルマウス (Q129 および Q113) を用いて、詳細な治療実験を行い、より顕著な疾患表現型を示す Q129 で、軽度ではあるが、体重減少抑制効果、rotarod test での運動機能改善効果を認めた。DRPLA protein の核内局在については、核移行シグナルを同定した。DRPLA protein の細胞内局在について、核移行シグナルを同定し、書くに存在するタンパクであること、核内では、核マトリックスに局在し、核マトリックスへの局在には、histone deacetylase 3 との結合が関与していることを見いだした。さらに、histone deacetylase 3 との結合により、DRPLA protein が安定化・不溶化することを明らかにした。

分担研究者

後藤順:東京大学医学部附属病院神経内科講師

岩田淳:東京大学大学院医学系研究科分子脳病態科学 特任准教授

伊達英俊:東京大学医学部附属病院神経内科 特任助教

佐藤俊哉:新潟大学脳研究所 実験動物学(動物資源開発研究分野) 助教

A 研究目的

本研究は、代表的な神経変性疾患であるポリグルタミン病を対象に、病因遺伝子産物の生理的機能を解明し、その知見に基づき分子病態機序を明らかにし、その上で、有効な治療法の対象となる分子標的を定め、分子標的治療

法を実現することを目的としている。ポリグルタミン病の対象疾患として、日本人に多い歯状核赤核・淡蒼球ルイ体萎縮症(dentatorubral-pallidoluyian atrophy, DRPLA)を取り上げ、その病因遺伝子産物(DRPLA タンパク)の機能解析、ヒトの病態をよく反映する動物モデルを用いた病態機序解析などに基づき、分子標的治療の研究を進める

これまでの研究で、ポリグルタミン病の本質的な病態機序は、時間依存性、CAG リピート長依存性で、部位特異的に生じる、変異 DRPLA タンパクの神経細胞の核内集積、その結果として生じる核の機能障害(basal level の転写障害および、転写活性化の障害)にあることを明らかにしている。

DRPLA の治療研究を進める上で、1.

DRPLA タンパクの核内の存在様式, 安定化の機構を明らかにすること, 2. DRPLA タンパクの核移行の機構の解明, 3. DRPLA タンパクの核移行阻害をターゲットにした cell-based assay system の確立と, この系を用いた化合物の探索, 4. 見出された, 核移行阻害剤について, モデル動物を用いた治療研究を進めること. 以上の4点について, 研究を進めてきた. 本年度は, これまでに見いだした核移行を阻害する物質について, 既に当研究室で確立している, DRPLA モデルマウスである, Q129, Q113 を用いた治療効果の検討を進めた. DRPLA protein の核移行については, 核移行の機序の研究, さらに, 核内での局在機構の解明を進めた.

B 研究方法

DRPLA モデルマウス (Q129, Q113) に対する経口投与実験

候補化合物の中から, 中枢神経系への移行が確認されている薬剤を選択して DRPLA モデルマウス (Q129, Q113) に対する経口投与実験を行った. DRPLA トランスジェニックマウス Q129 及び Q113 に対し 5 週齢から経口投与を開始した. 化合物濃度はこれまでの研究で効果が示唆された 30ppm (Q129:23 匹, Q113:33 匹)と, 対照として 0ppm (Q129:22 匹, Q113:33 匹)を選択した. 治療効果は各群の体重, 餌の摂取量, rotarod test 及び open field test による運動機能評価, 生存期間により判定した.

DRPLA protein の核内局在機構に関する実験

これまでに見出した, DRPLA タンパクと結合するタンパクについて, GFP-DRPLA タンパクの定常発現株にトランスフェクションにより発現させ, DRPLA タンパクの核マトリックスへの局

在に対して影響を与えるかどうかの検討を行った.

C 研究結果

DRPLA モデルマウス (Q129 および Q113) に対する経口投与実験

低分子化合物ライブラリーのスクリーニングで同定された 34 種類の中の1つについて, DRPLA モデルマウス (Q129 および Q113) を用いて, 化合物濃度 30 ppm について個体数を増やした詳細な検討を行った. より顕著な疾患表現型を示す Q129 では, 軽度ではあるが, 体重減少抑制効果, rotarod test での運動機能改善効果を認めしたが, より軽度の疾患表現型を示す Q113 では, その効果は明確ではなかった.

今後よりリピート数の少ない Q96 マウスを用いた実験や, 記憶等他の疾患表現型に対する治療効果をみることを検討している. また, 他の化合物の治療効果に関しても順次検討していく必要がある.

DRPLA protein の核内局在機構に関する実験

これまで, DRPLA protein と結合するタンパクを多数見出しているタンパクについて, GFP-DRPLA タンパクの定常発現株にトランスフェクションにより発現させ, DRPLA protein の核内局在を変化させるかどうかについて検討した. その結果, histone deacetylase 3 (HDAC3) を発現させると, DRPLA タンパクの核マトリックスへの移行が促進されることを見いだした. このことにより, DRPLA protein の安定化と不溶化が促進されることを見いだした. さらに, HDAC3 について, さまざまな長さの deletion mutant を作成し, DRPLA protein との結合部位についての詳細な解析を行った結果,

DRPLA protein と結合する HDAC3 内の部位を
同定した。

D 考察

DRPLA モデルマウス (Q129 および Q113)
に対する経口投与実験については、見出した
34 種類の化合物のうち、1 つについて、治療実
験を完了した。軽度の改善が見られたものの、
さらに治療効果の期待できる薬物があるかど
うかについて、他の化合物についても治療実
験を進める必要がある。モデル動物を用いた
治療研究は、長期の時間と飼育設備を必要と
するので、効率の良い治療実験の推進のため
には、大規模な治療実験ができる体制の準備
が必要であり、アカデミアの研究を支援する体
制の構築が望まれる。

DRPLA タンパクの核内局在機構に関する
研究については、HDAC3 が、DRPLA タンパク
の核マトリックスへの局在に重要な役割を果た
していることを見出した。この発見は、変異
DRPLA タンパクの核内集積の機序に関連する
という点で重要であると評価できる。さらに、核
マトリックスへの局在を阻害することにより、核
内集積を抑制できる可能性があり、新たな治
療の分子標的としても評価できる。

E 結論

DRPLA の病態機序として、変異 DRPLA タン
パクの核移行、核内集積、核の機能障害が重
要であることを見出した。DRPLA タンパクが
HDAC3 と結合して核マトリックスに局在し、安
定化すること、核マトリックスへの局在の阻害
が新たな治療ターゲットになることを見出した。
DRPLA タンパクの核移行の阻害に焦点を当て、
cell-based assay system を構築し、アメリカ食
品医薬品局 (FDA) により米国で臨床試験にま

で到達した化合物のライブラリー (1040 種類の
化合物) をスクリーニングし、核移行を阻害す
る、あるいは、核内局在を変化させる化合物と
して 34 種類見出したが、これらの化合物の中
の 1 つについて、DRPLA モデル動物を用いた
投与実験を行い、軽度ではあるが、運動機能
の改善効果を見出した。今後、他の化合物に
ついては、その治療効果を確認していく必要が
ある。

F 健康危険情報

該当なし。

G 研究発表

1 論文発表

Suzuki K, Zhou J, Sato T, Takao K,
Miyagawa T, Oyake M, Yamada M,
Takahashi H, Takahashi Y, Goto J, and
Tsuji S. DRPLA transgenic mouse
substrains carrying single copy of
full-length mutant human DRPLA gene
with variable sizes of expanded CAG
repeats exhibit CAG repeat length- and
age-dependent changes in behavioral
abnormalities and gene expression profiles.
Neurobiol. Dis. 46: 336-350, 2012

2 学会発表

なし

H 知的財産権の出願・登録状況

1. 特許取得

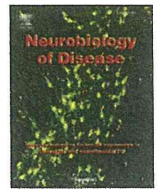
2. 実用新案登録

3. その他



Contents lists available at SciVerse ScienceDirect

Neurobiology of Disease

journal homepage: www.elsevier.com/locate/ynbdi

DRPLA transgenic mouse substrains carrying single copy of full-length mutant human DRPLA gene with variable sizes of expanded CAG repeats exhibit CAG repeat length- and age-dependent changes in behavioral abnormalities and gene expression profiles

Kazushi Suzuki^{a,1}, Jiayi Zhou^{a,1,2}, Toshiya Sato^b, Keizo Takao^{e,f,g}, Tsuyoshi Miyagawa^{e,f,g}, Mutsuo Oyake^{c,3}, Mitunori Yamada^d, Hitoshi Takahashi^d, Yuji Takahashi^a, Jun Goto^a, Shoji Tsuji^{a,*}

^a Department of Neurology, The University of Tokyo, Bunkyo-ku, Tokyo, 113-8655, Japan

^b Center for Bioresource-Based Research, Brain Research Institute, Niigata University, Niigata, 951-8585, Japan

^c Department of Neurology, Brain Research Institute, Niigata University, Niigata, 951-8585, Japan

^d Department of Pathology, Brain Research Institute, Niigata University, Niigata, 951-8585, Japan

^e Section of Behavior Patterns, Center for Genetic Analysis of Behavior, National Institute for Physiological Sciences, Okazaki, 444-8585, Japan

^f Frontier Technology Center, Graduate School of Medicine, Kyoto University, Kyoto, 606-8501, Japan

^g Division of Systems Medicine, Institute for Comprehensive Medical Science, Fujita Health University, Aichi, 470-1192, Japan

ARTICLE INFO

Article history:

Received 14 June 2011

Revised 31 December 2011

Accepted 26 January 2012

Available online xxxxx

Keywords:

Dentatorubral-pallidolusian atrophy

DRPLA transgenic mice

Neurodegeneration

Polyglutamine

Expression profiling

Microarray

Behavioral abnormality

Transcriptional dysregulation

Calcium signaling

Neuropeptides

ABSTRACT

Dentatorubral-pallidolusian atrophy (DRPLA) is an autosomal dominant progressive neurodegenerative disorder with intellectual deterioration and various motor deficits including ataxia, choreoathetosis, and myoclonus, caused by an abnormal expansion of CAG repeats in the DRPLA gene. Longer expanded CAG repeats contribute to an earlier age of onset, faster progression, and more severe neurological symptoms in DRPLA patients. In this study, we have established DRPLA transgenic mouse lines (sublines) harboring a single copy of the full-length mutant human DRPLA gene carrying various lengths of expanded CAG repeats (Q76, Q96, Q113, and Q129), which have clearly shown motor deficits and memory disturbance whose severity increases with the length of expanded CAG repeats and age, and successfully replicated the CAG repeat length- and age-dependent features of DRPLA patients. Neuronal intranuclear accumulation of the mutant DRPLA protein has been suggested to cause transcriptional dysregulation, leading to alteration in gene expression and neuronal dysfunction. In this study, we have conducted a comprehensive analysis of gene expression profiles in the cerebrum and cerebellum of transgenic mouse lines at 4, 8, and 12 weeks using multiple microarray platforms, and demonstrated that both the number and expression levels of the altered genes are highly dependent on CAG repeat length and age in both brain regions. Specific groups of genes and their function categories were identified by further agglomerative cluster analysis and gene functional annotation analysis. Calcium signaling and neuropeptide signaling, among others, were implicated in the pathophysiology of DRPLA. Our study provides unprecedented CAG-repeat-length-dependent mouse models of DRPLA, which are highly valuable not only for elucidating the CAG-repeat-length-dependent pathophysiology of DRPLA but also for developing therapeutic strategies for DRPLA.

© 2012 Elsevier Inc. All rights reserved.

Abbreviations: ANOVA, analysis of variance; CDK, cyclin-dependent kinase; CREB, cAMP response element-binding protein; DRPLA, dentatorubral-pallidolusian atrophy; GO, gene ontology; KO, knock-out; MAPK, mitogen-activated protein kinase; MJD, Machado–Joseph disease; NIA, neuronal intranuclear accumulation; nTg, nontransgenic; RT-PCR, Reverse transcription-polymerase chain reaction; SAHA, suberoylanilide hydroxamic acid; SBMA, spinal and bulbar muscular atrophy; SCA, spinocerebellar ataxia.

* Corresponding author. Fax: +81 358006844.

E-mail address: tsuji@m.u-tokyo.ac.jp (S. Tsuji).

¹ The first two authors (K. Suzuki and J. Zhou) are co-first authors who contributed equally to the work presented here.

² Present address: Department of Molecular and Cell Biology, Boston University Henry M. Goldman School of Dental Medicine, Boston University Medical Campus, Boston, MA 02118, USA.

³ Present address: Nagaoka Red Cross Hospital, Nagaoka 940-2085, Japan.

Available online on ScienceDirect (www.sciencedirect.com).

0969-9961/\$ – see front matter © 2012 Elsevier Inc. All rights reserved.

doi:10.1016/j.nbd.2012.01.014

Introduction

DRPLA is a progressive neurodegenerative disease with autosomal dominant inheritance that is caused by an abnormal expansion of CAG repeats in the coding region of the DRPLA gene at 12p13.31, which encodes an abnormally expanded polyglutamine tract in the DRPLA protein (also called atrophin-1) (Koide et al., 1994; Nagafuchi et al., 1994). The diseases caused by this mechanism are called polyglutamine diseases, which so far, besides DRPLA, include spinal and bulbar muscular atrophy (SBMA) (La Spada et al., 1991), Huntington's disease (The Huntington's Disease Collaborative Research Group, 1993), spinocerebellar ataxia type 1 (SCA1) (Orr et al., 1993), SCA2 (Imbert et al., 1996; Pulst et al., 1996; Sanpei et al., 1996), Machado–Joseph disease

Please cite this article as: Suzuki, K., et al., DRPLA transgenic mouse substrains carrying single copy of full-length mutant human DRPLA gene with variable sizes of expanded CAG ..., Neurobiol. Dis. (2012), doi:10.1016/j.nbd.2012.01.014

(MJD/SCA3) (Kawaguchi et al., 1994), SCA6 (Zhuchenko et al., 1997), SCA7 (David et al., 1997; Lindblad et al., 1996), and SCA 17 (Koide et al., 1999; Nakamura et al., 2001). DRPLA patients show wide varieties of progressive neurological deficits depending on the age at onset (Naito and Oyanagi, 1982). The patients with earlier onset (younger than 20 years old) present a progressive phenotype characterized by intellectual deterioration, behavioral changes, ataxia, myoclonus, and epilepsy, whereas the patients with later onset characteristically show cerebellar ataxia, choreoathetosis, dementia, and character changes. The age at onset inversely correlates with the CAG repeat length in the mutant allele of the DRPLA gene (Ikeuchi et al., 1995; Koide et al., 1994; Nagafuchi et al., 1994).

Although the physiological functions of the DRPLA protein are not yet fully understood, recent studies have shown that it localizes in the nucleus (Sato et al., 2009; Sato et al., 1999a; Wood et al., 2000), functions as a transcription coregulator (Shen et al., 2007; Wood et al., 2000; Zhang et al., 2002), and plays a role in multiple developmental processes (Erkner et al., 2002; Zhang et al., 2002). Mutant proteins with abnormally expanded polyglutamine tracts have been shown to interact with coactivators of cAMP-responsive element-binding protein (CREB)-dependent transcription, such as TAF_{II}130 (Shimohata et al., 2000) and CBP (Nucifora et al., 2001), leading to transcriptional dysregulation.

Neuropathological changes in DRPLA are conventionally considered to be mainly due to the degeneration of both the dentatorubral and pallidolusian systems, characterized by neuronal loss associated with astrogliosis. However, recent studies have revealed that the neuronal intranuclear accumulation (NIA) of mutant DRPLA proteins is a pathological hallmark in the brains of both DRPLA patients and transgenic mice, which appears in CAG-repeat-length-dependent, age-dependent, and region-specific manners, with regional involvement far beyond the dentatorubral and pallidolusian systems (Sato et al., 2009; Yamada et al., 2001).

In this study, we sought to establish transgenic mouse models that closely reproduce the pathophysiologic processes in the brain of patients with DRPLA in order to provide valuable tools for further elucidation of the pathogenetic mechanisms of the disease. To realize this aim, we inserted a full-length mutant human DRPLA gene carrying expanded CAG repeats under the control of its own promoter. We initially established a mouse strain (Q76) that carried a single copy of the full-length human DRPLA gene with a mildly expanded CAG repeat length (76 repeats) (Sato et al., 1999b). The Q76 mice, however, did not exhibit obvious neurological phenotypes. Owing to intrinsic instabilities of expanded CAG repeats, we serendipitously generated transgenic mice carrying highly expanded 129 CAG repeats (Q129), which showed severe neurological phenotypes resembling those observed in juvenile-onset DRPLA patients carrying largely expanded CAG repeats (Sato et al., 2009). Subsequently, we were able to generate another two DRPLA transgenic mouse strains carrying different lengths of CAG repeats (113 and 96) from the Q129 mouse strain. Taken together, one whole set of DRPLA transgenic mouse strains (Q76, Q96, Q113, and Q129) have been established. These mouse strains should be ideal models for investigating CAG-repeat-length-dependent pathologies because of their two distinctive characteristics. One is that the transgene is driven by its own promoter and expressed within a physiologically relevant level [approximately 80% of the expression level of the endogenous DRPLA gene (Sato et al., 2009)]. The other is that the four transgenic strains are genetically identical (the same integration site for the expanded CAG repeats in the DRPLA gene) except for the CAG repeat length. Hence, the size of the expanded CAG repeats in the transgene is considered to be solely responsible for the CAG-repeat-length-dependent phenotypic variation across the Q76, Q96, Q113, and Q129 transgenic strains, whose genetic difference only lies in the length of the expanded CAG repeats. To investigate the effects of the different sizes of expanded CAG repeats on the pathophysiologic mechanisms caused by expanded polyglutamine stretches, we have conducted detailed evaluations of the phenotypic differences in these transgenic mice and

the expression profiles of mRNAs in the brains of these transgenic mice. Here, we report that differences in the phenotypic and expression profiles are closely influenced by the size of expanded CAG repeats as well as disease duration.

Materials and methods

All animal experiments were performed in accordance with the National Institutes of Health Guide for the Care and Use of Laboratory Animals. All behavioral analyses except the Barnes maze test were performed in the University of Tokyo. The Barnes maze test was performed in the Graduate School of Medicine, Kyoto University. Mice were housed in a room with a 12-hour light/dark cycle (lights on at 6:00 a.m. in the University of Tokyo, at 7:00 a.m. in Kyoto University) with access to food and water *ad libitum*. The behavioral phenotype data obtained by a comprehensive behavioral test battery (Yamasaki et al., 2008) conducted in Kyoto University, which are not described in this article, can be found in the gene-brain-phenotyping database (<http://www.mouse-phenotype.org/>).

Generation of DRPLA transgenic mice

The generation of Q76 and Q129 DRPLA transgenic mice was previously described (Sato et al., 2009; Sato et al., 1999b). Because DRPLA transgenic mice are difficult to reproduce naturally, they were propagated by *in vitro* fertilization. The sperms of hemizygous transgenic mice were used to back fertilize the eggs of C57BL/6J mice. The fertilized eggs were transplanted to surrogate mother mice, and grown mice were weaned 20 days after birth. The genotypes of the transgenics were identified by PCR analysis of tail DNA using two protocols. In one PCR protocol, to detect the human-derived transgene, genomic DNA was amplified using the primer pair of h/mDRPLASerstretchF (5'-CTGCCCTGAGACCCCTCAAC-3') and h/mDRPLASerstretchR (5'-FAM-TGGGATGGGAGAGAAGGCTG-3'), which enables the simultaneous amplification of both human and mouse DRPLA genes. Taking advantage of the difference in the length of the serine stretch between the human DRPLA gene (*ATN1*) and the mouse DRPLA gene (*Atn1*), the 391 bp fragment derived from the human DRPLA gene and the 382 bp fragment derived from the murine orthologue were easily identified. After the initial denaturation at 94 °C for 2 min, PCR was performed for 30 cycles consisting of denaturation at 94 °C for 30 s, annealing at 60 °C for 30 s, and extension at 68 °C for 60 s, followed by a final extension at 68 °C for 10 min. In the other PCR protocol, only the human mutant fragment containing the expanded CAG repeats was amplified using the primer pair of DR1589F (5'-FAM-CACCAGCTCAACATCACCATC-3') and DR1825R (5'-AGGACACCTGGCTGTGAGGT-3'). After the initial denaturation at 95 °C for 2 min, PCR was performed for 35 cycles consisting of denaturation at 98 °C for 10 s, annealing at 55 °C for 30 s, and extension at 60 °C for 60 s, followed by a final extension at 72 °C for 7 min. The fragment analysis of PCR products was accomplished using an ABI 3100 genetic analyzer and Genemapper v3.5 software (Applied Biosystems, Foster City, CA, USA).

Analysis of phenotypes

Body weight was measured on Monday morning every two weeks. Behavioral analyses were performed during when the lights were on. After each test, all the apparatuses used were washed with water followed by 70% ethanol or super-hypochlorous water to remove the smell of mice. Mice were assessed for morbidity and mortality daily.

Accelerating rotarod test

An accelerating rotarod apparatus (O'Hara Co., Ltd., Tokyo, Japan) was used to measure forehand and hindlimb motor coordination and balance. The rod has a diameter of 3 cm and is covered with rubber. Mice were placed on a rotating rod (3.5 rpm), and the rotation

speed was linearly increased to 35 rpm within a period of 300 s and maintained at 35 rpm until 600 s. The latency to fall off or to cling to the rod within the determined time period was recorded. Mice underwent three trials per day and the maximum latency was used in subsequent analyses.

Beam walking test

The beam walking apparatus (O'Hara Co., Ltd., Tokyo, Japan) consisted of a 1-m-long beam with a round cross section, which was placed horizontally 50 cm above the floor, and a safe platform at one end. A lamp was positioned such that it provided bright illumination at the starting end of the beam. In each test, a mouse was placed on the beam at the starting end, and the amount of time required for the mouse to walk across the beam was recorded. The test was conducted over three consecutive days. Mice were trained during the first 2 days to cross the beam to the safe platform on the opposite side. On the third day, each mouse underwent three trials, and the minimum time was used in subsequent analyses. Mice were allowed a maximum of 90 s to cross the beam. Mice were returned to their individual home cages between trials.

Open field test

The open field was a 50 cm square white floor with 40-cm-high transparent walls, illuminated by a 70 lx LED light placed above the field. The entire apparatus was placed in a soundproofed box. The horizontal and vertical movements of individual mice were monitored by a camera placed above the field and a photobeam sensor placed 7 cm from the field. Field images were captured every 0.5 s and the difference between two sequenced images was measured as the moving distance of the mouse. In each test, the mouse to be tested was placed in a fixed corner of the field and its spontaneous behavior was monitored for 10 min. Captured images and photobeam sensor interruption data were analyzed on a Macintosh computer using Image OF circle 1.01× (O'Hara Co., Ltd., Tokyo, Japan), a modified software platform from the public domain NIH image program (<http://rsb.info.nih.gov/nih-image/>). The field was conceptually divided into 25 square sections (10×10 cm²) in image analysis. Total moving distance (cm) and the frequency of rearings (determined by counting the number of photobeam interruptions) were recorded.

Barnes maze test

The Barnes maze was conducted on "dry land", a white circular surface, 1.0 m in diameter, with 12 holes equally spaced around the perimeter (O'Hara Co., Ltd., Tokyo, Japan). The circular surface was elevated 75 cm from the floor. A black Plexiglass escape box (17×13×7 cm³), which had paper cage bedding on its bottom, was located under one of the holes. The hole above the escape box represented the target. The location of the target was consistent for a given mouse but randomized across mice. The maze was rotated daily, with the spatial location of the target unchanged with respect to the distal visual room cues, to prevent a bias based on olfactory or proximal cues within the maze. Three trials per day were conducted during the training session. Twenty-four hours after the 18th training, a probe trial was conducted without the escape box to confirm that this spatial task was learned on the basis of navigation by distal environmental room cues. Another probe trial was conducted 1 week after the initial probe test to evaluate memory retention. Three days after the memory retention test, the escape box was moved to a new position opposite to the original for reversal learning. Mice were then subjected to 15 consecutive trials to locate the new position of the escape box using the same procedure as described above. The time spent around each hole was recorded using Image BM software, a modified software platform from the public domain NIH image program.

Expression profile analysis

The Q76, Q113, Q129, and nontransgenic (nTg) mice were sacrificed at 4, 8, and 12 weeks of age. Three littermates were assigned to each group. Mice were euthanized by cervical dislocation. The brain was immediately removed and separated into the cerebrum and cerebellum on ice. They were immediately frozen with dry ice and deep-frozen at −80 °C. Total RNA was extracted from the tissue using TRIZOL reagent (Invitrogen, Carlsbad, CA, USA) in accordance with the manufacturer's instructions. PolyA(+) RNA was isolated from 25 µg of total RNA using an oligotex-dT30 mRNA purification kit (Takara Bio Inc., Shiga, Japan).

For the single-colored array experiments (Genechip mouse expression set 430 A and B, Affymetrix, Santa Clara, CA, USA), 200 ng of polyA(+) RNA was used for cRNA synthesis by one-cycle amplification. Twenty micrograms of cRNA was fragmented and hybridized with the array. Washing and scanning were performed using Affymetrix Fluidics Station 450 in accordance with the manufacturer's instructions. The arrays were scanned with an Affymetrix Gene Array Scanner using Affymetrix Genechip Operating Software.

In the two-colored array experiments (mouse 22K oligo array G4121A, Agilent, Santa Clara, CA, USA), 125 ng of polyA(+) RNA was used for cRNA synthesis, and cRNA was labeled with Cy3 or Cy5. One microgram of Cy3-labeled cRNA and the same amount of Cy5-labeled cRNA were fragmented and hybridized with the array. After washing, the arrays were scanned using an Agilent DNA microarray scanner and Agilent feature extraction software ver. 8.1.

Reverse transcription-polymerase chain reaction (RT-PCR)

The expression levels of transgenes in the brains of transgenic mice were analyzed by RT-PCR as described previously (Sato et al., 1999b).

Statistical analyses

Statistical analyses of data on body weight and data from the rotarod test, beam walking test, open field test, and Barnes maze test were performed by two-way or one-way ANOVA followed by the post hoc test when appropriate. The difference between the average time spent around the target hole and that spent around the adjacent holes in the probe test in the Barnes maze was evaluated using the paired *t*-test. Survival data were analyzed using the Kaplan–Meier method and compared by the log-rank test. A *p*-value of ≤0.05 was considered significant. Data are shown as means ± SEM.

Statistical analysis of all microarray data was performed using Rosetta Resolver ver. 6.0 (Rosetta Biosoftware, Kirkland, WA, USA). The software produces intensity or ratio profiles from imported scanned data using a processing pipeline that includes preprocessing (background correction and intrachip normalization) and postprocessing of data and error model adjustments. It also produces intensity experiment profiles or ratio experiment profiles combining replicates in an error-weighted manner. For single-color experiment data, Ratio Builder was used to calculate fold changes and ratio *p*-values. Detailed information about the Affymetrix Genechip error model and Ratio Building error model in the Rosetta Resolver system can be found at <http://www.rosettatabio.com/tech>. Gene annotation analysis was performed using a DAVID (<http://david.abcc.ncifcrf.gov/>) annotation tool. Statistically overrepresented GO terms and KEGG pathways were identified on the basis of a modified Fisher exact *p*-value, that is, EASE score (≤0.05) calculated using DAVID (Dennis et al., 2003; Huang da et al., 2009) (<http://david.abcc.ncifcrf.gov/>).

Results

Behavioral analysis revealed significant CAG-repeat-length-dependent changes in neurological phenotypes of Q76, Q96, Q113, and Q129 DRPLA transgenic mice

The lifespan of each transgenic mouse line is demonstrated as a Kaplan–Meier curve in Fig. 1A. The survival time of the mouse lines clearly decreased as the CAG repeat length increased in the transgene. The median survival times of Q129, Q113, Q96, Q76, and nTg mice were 75, 208.5, 589.5, 830.5, and 891 days, respectively. The Q76 mice survived for over two years, but their survival time was significantly shorter than that of nTg mice ($p = 0.045$ by log-rank test). The gain of body weight in the transgenic mice over time was significantly impaired as CAG repeat length increased (Fig. 1B). The time of onset of weight loss was also found to be dependent on CAG repeat length. Significant body weight loss occurred as early as 6 weeks of age in the Q129 mice ($p < 0.001$), earlier than in other transgenic strains. The body weights of the Q113, Q96, and Q76 transgenic strains were initially the same as that of the nTg mice, but a significant body weight loss was observed from 20, 42, and 48 weeks of age in the Q113, Q96, and Q76 strains, respectively ($p < 0.05$).

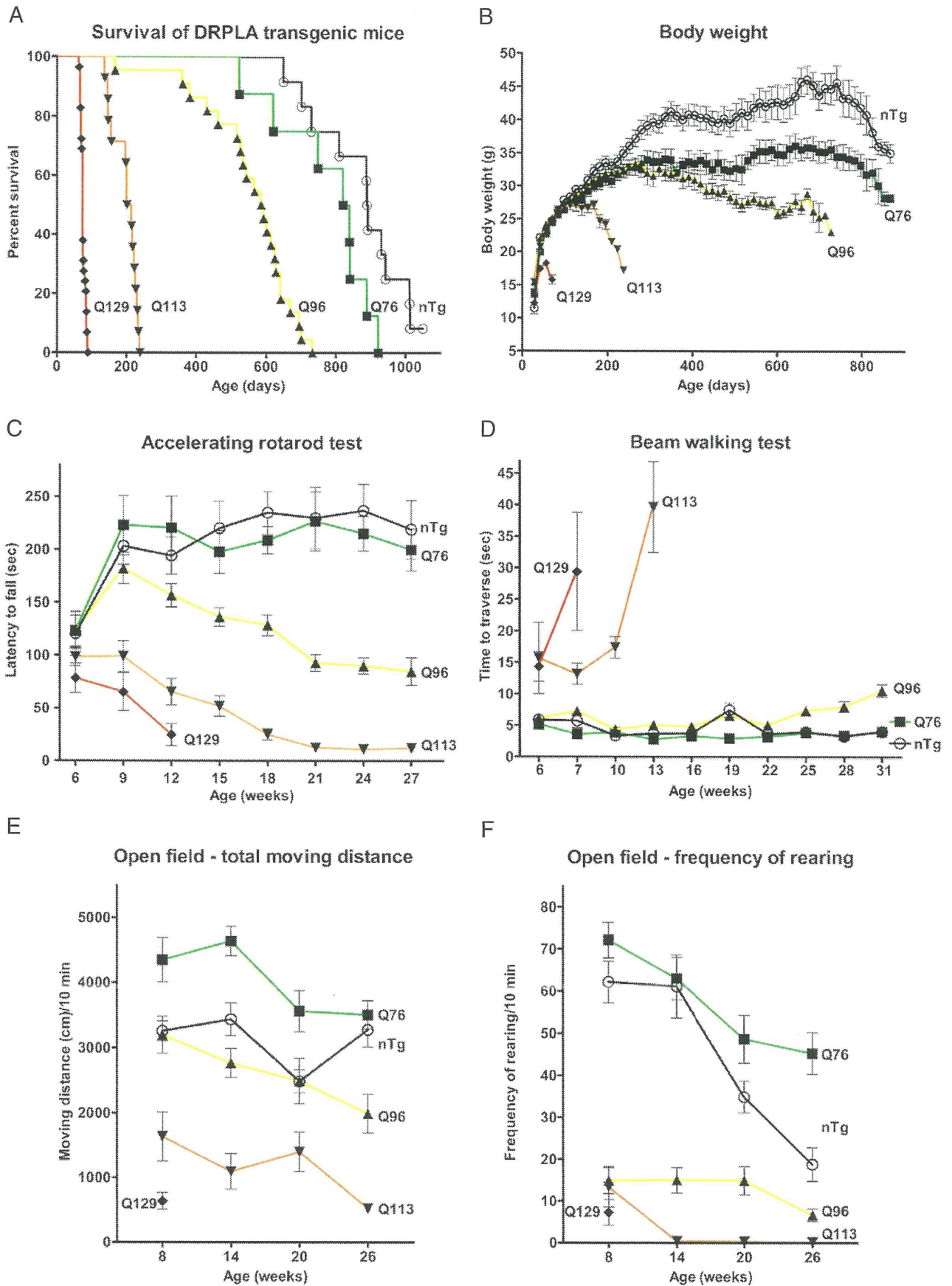
Motor coordination and balance were assessed using the accelerating rotarod test (Fig. 1C). The nTg mice showed daily and weekly increases in latency to fall off following training over time and showed stable performance in remaining on the rotating rod from 12 weeks of age. The performance of the Q76 mice was not significantly different from that of the nTg mice (nTg vs Q76: $F_{1,112} = 0.22$, $p = 0.6371$), although it seemed to slightly decline from 24 weeks of age, which was not statistically significant. By contrast, the Q96, Q113, and Q129 strains showed poor performance and a progressive decrease in latency to fall off the rotating rod in a CAG-repeat-length-dependent manner. The Q129 mice showed a marked decrease in latency to fall off after 9 weeks of age ($p < 0.001$), and at approximately 12 weeks of age they could not even hang onto the rod (nTg vs Q129: $F_{1,39} = 69.43$, $p < 0.0001$). The Q113 mice also showed a significant decrease in latency to fall off from 9 weeks of age ($p < 0.01$), which however was milder and progressed more slowly than in the Q129 mice (nTg vs Q113: $F_{1,107} = 300.69$, $p < 0.0001$). The Q96 mice seemed to show slight decline in performance on the rotarod from 9 weeks of age, but the decrease in latency to fall off did not reach statistical significance until 18 weeks of age ($p < 0.01$, nTg vs Q96: $F_{1,112} = 81.92$, $p < 0.0001$). The abnormalities in motor coordination and balance of the Q129, Q113, Q96, and Q76 strains were also assessed by the beam walking test (Fig. 1D). The ability of rodents to traverse a stationary horizontal rod is assumed to measure both sensorimotor coordination and the integrity of the vestibular sensory system (Carter et al., 1999). The Q129 and Q113 mice had progressively increasing difficulty in traversing the beam from a very early age, and became incapable of completing the task from 10 to 16 weeks, respectively. The Q96 mice were able to

complete the task within the determined time window (90 s) throughout the observation period, but their performance was significantly worse than that of the nTg mice (nTg vs Q96: $F_{1,140} = 50.62$, $p < 0.0001$). By contrast, the performance of Q76 mice was not impaired and even showed better performance than nTg mice at all time points examined (nTg vs Q76: $F_{1,140} = 13.85$, $p = 0.0003$) except at 10 and 28 weeks, indicating that motor coordination was not impaired in the Q76 mice.

Spontaneous locomotor behavior was monitored using the open field test at 8, 14, 20, and 26 weeks of age for all the strains except the Q129 strain, because the Q129 mice could not complete the open field task after 8 weeks of age. Horizontal activity was evaluated by the total moving distance (cm) that the mouse traveled during a 10 min period (Fig. 1E). As early as 8 weeks of age, the Q129 mice showed severe dysfunction in horizontal movement and moved less than 1000 cm during the 10 min test period. The total moving distance of the Q113 mice was much shorter than those of the Q96 and Q76 mice even at 8 weeks, and tended to decrease thereafter. The total moving distance of the Q96 mice was not significantly different from that of the nTg mice at 8 weeks of age, but thereafter it gradually decreased with age. On the other hand, the total moving distance of the Q76 mice was significantly longer than that of the nTg mice until 20 weeks of age (nTg vs Q76: $F_{1,55} = 25.86$, $p < 0.0001$; $p < 0.05$ at 8 weeks, $p < 0.01$ at 14 weeks, and $p < 0.05$ at 20 weeks), suggesting that hyperactivity in exploratory behavior at early ages is a characteristic behavioral change in the Q76 mice. Vertical activity was assessed by the frequency of rearing (Fig. 1F). Rearing is the standing of animals on their hindlimbs with the forelimbs up in the air, which is considered to reflect a reaction to a novel environment. The Q129 mice could barely rear as early as 8 weeks of age. The Q113 and Q96 mice also showed inability to rear from an early age (8 weeks), whereas the horizontal activity of the Q96 mice did not decrease at this age. This finding may reflect the fact that the rearing movement requires higher levels of motor skills and muscular power than horizontal movements. As in the case of horizontal activity, the Q76 mice showed a higher frequency of rearing than the nTg mice.

To exclude the possibility that the differences in behavioral phenotypes among the Q76, Q96, Q113, and Q129 mice were caused by the differences in the expression levels of transgenes, we analyzed the mRNA levels of the mutant human DRPLA transgenes in the brains of Q76, Q96, Q113, and Q129 mice by competitive RT-PCR, which enables simultaneous quantification of the human transgene and endogenous mouse DRPLA gene. The mRNA levels of the mutant human DRPLA transgenes in these transgenic mice were determined to be all at ~80% of those of the endogenous mouse DRPLA gene (Supplementary Fig. 1). This finding indicates that the differences in the phenotypes among the Q76, Q96, Q113, and Q129 mice were not caused by the differences in the expression levels of the transgenes but by the differences in the CAG repeat lengths of the transgenes.

Fig. 1. Phenotypes and behavioral analyses of DRPLA transgenic mouse strains. Squares, triangles, inverse triangles, diamonds, and open circles indicate the Q76, Q96, Q113, Q129, and nTg mouse strains, respectively. Data on body weight and accelerating rotarod test results include some missing values because of death of mice, which are excluded from statistical analysis. A. Kaplan–Meier curve of DRPLA transgenic and nTg mice. The median survival times of Q129 ($n = 29$), Q113 ($n = 14$), Q96 ($n = 22$), Q76 ($n = 8$), and nTg ($n = 11$) mice were 75, 208.5, 589.5, 830.5, and 891 days, respectively. B. Body weight of DRPLA transgenic and nTg mice. Symbols indicate the means \pm SEM of body weight (g) of Q76 ($n = 8$), Q96 ($n = 22$), Q113 ($n = 16$), Q129 ($n = 23$), and nTg ($n = 18$). C–F. Behavioral analyses. The time points of data acquisition were shown in horizontal axis. C. Accelerating rotarod test. This figure shows significant age- and CAG-repeat-length-dependent changes in the performance of the DRPLA transgenic mice in the accelerating rotarod test. Symbols indicate the means \pm SEM of latency (sec) to fall of the Q76 ($n = 8$), Q96 ($n = 8$), Q113 ($n = 8$), Q129 ($n = 7$) and nTg ($n = 8$) mice. D. Beam walking test. This figure shows significant age- and repeat-length-dependent changes in the performance of the DRPLA transgenic mice in the beam walking test. Symbols indicate the means \pm SEM of time (sec) to cross the beam ($n = 8$) of the Q76, Q96, Q113, Q129, and nTg mice. E. Open field test – horizontal activity. The horizontal activity of the Q76, Q96, Q113, Q129, and nTg mice in the open field test is shown as the total moving distance (cm) during a test period of 10 min. Data are shown as the means \pm SEM ($n = 8$). F. Open field test – vertical activity. The vertical activity of the Q76, Q96, Q113, Q129, and nTg mice in the open field test is shown as the frequency of rearing (number of times) during a test period of 10 min. Data are shown as the means \pm SEM ($n = 8$). G–K. Barnes maze test: The Barnes maze test was conducted using Q76 ($n = 9$), Q96 ($n = 10$), and nTg ($n = 10$) mice. The first special acquisition, the probe test 24 h after the last training, the probe test 7 days after the last training, the reversal learning, and the probe test after reversal learning were serially performed at 23, 25, 26, 27, and 28 weeks of age, respectively. The results were shown as the means \pm SEM. G. Barnes maze test – latency to reach target. The latency to reach the target is significantly increased in Q96 mice, whereas Q76 did not show an increased latency to reach the target. H. Barnes maze test – probe test 24 h after last training. Discrimination of the target from the neighboring locations was clearly impaired in Q76 and Q96 mice. I. Barnes maze test – probe test 7 days after last training. Discrimination of the target from the neighboring locations was significantly impaired only in Q96 mice. J. Barnes maze test – reversal learning. The latency to the target significantly increased in Q96 mice. K. Barnes maze test – probe test after reversal learning. Discrimination of the target from both the neighboring locations and original target was impaired in Q96 mice.



Please cite this article as: Suzuki, K., et al., DRPLA transgenic mouse substrains carrying single copy of full-length mutant human DRPLA gene with variable sizes of expanded CAG ..., *Neurobiol. Dis.* (2012), doi:10.1016/j.nbd.2012.01.014

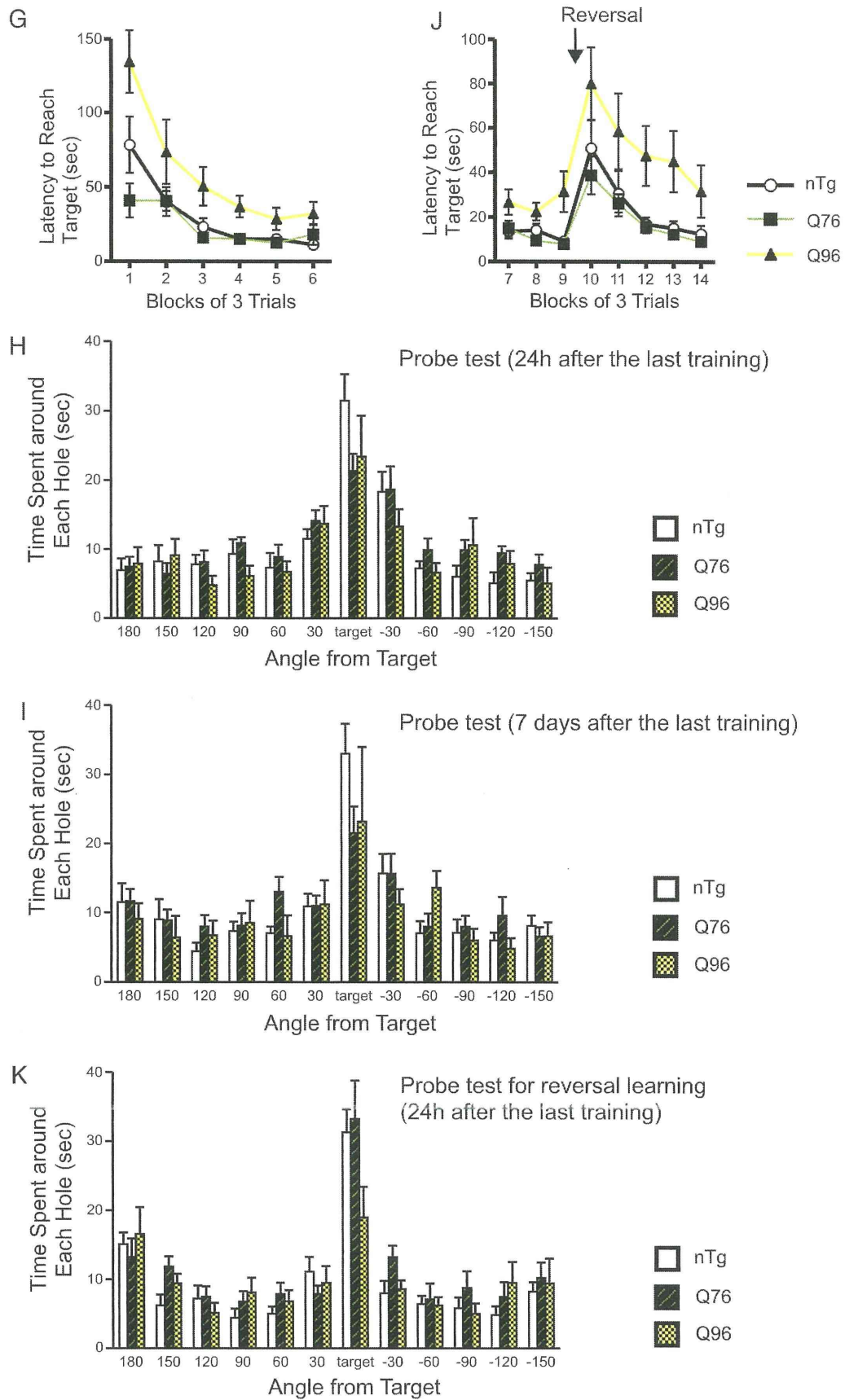


Fig. 1 (continued).

The transgenic mice with mildly expanded CAG repeats show deficits in spatial learning and reference memory

We performed detailed analyses focusing on the learning and memory of Q76 and Q96 mice, which show only mild deficits in the horizontal activity. Figs. 1G–K showed the results of Barnes maze test. In spatial memory acquisition, the latency to reach the target is significantly delayed in Q96 mice, indicating learning disability (Q96 vs nTg: $p < 0.01$), whereas Q76 mice did not show an increased latency to reach the target (Q76 vs nTg: $p = 0.5254$) (Fig. 1G, genotype effect: $F_{2,26} = 4.731$, $p = 0.179$). In the probe test 24 h after the last training, discrimination of the target from the neighboring locations is clearly impaired in the Q76 mice (target vs adjacent holes: $t_9 = 1.897$, $p = 0.0944$) and Q96 mice (target vs adjacent holes: $t_9 = 1.616$, $p = 0.1406$), whereas nTg mice were able to discriminate the target (target vs adjacent holes: $t_9 = 4.542$, $p < 0.01$) (Fig. 1H). Q76 and Q96 mice traveled longer distance to reach the target than Q76 although total moving distance was not significantly different among Q76, Q96, and nTg mice, supporting that the result was not attributable to the motor impairment of the Q76 and, in particular, the Q96 mice (Supplementary Figs. 2A, B). In the probe test 7 days after the last training, discrimination of the target from the neighboring locations is impaired only in the Q96 mice (target vs adjacent holes: $t_9 = 1.138$, $p = 0.2844$) (Fig. 1I). The distance to reach the target of Q96 mice was also significantly larger than those of other two strains (Supplementary Figs. 2C, D). A similar learning disability was also confirmed in the Q96 mice by the reversal learning (genotype effect: $F_{2,26} = 4.713$, $p = 0.0179$; Q96 vs. nTg: $p = 0.0213$) (Fig. 1J) and probe test (new target vs. previous target: $t_9 = 0.364$, $p = 0.7242$) (Fig. 1K and Supplementary Figs. 2E, F). These findings suggest that the Q96 mice showed impairment in spatial learning, short-term reference memory, and long-term reference memory, whereas the Q76 mice showed much milder phenotypes than the Q96 mice.

Expression profile analysis using multiple platforms revealed CAG-repeat-length- and age-dependent changes in the numbers of both upregulated and downregulated genes in the brains of the DRPLA transgenic mice

Affymetrix platform

To clarify how transcriptional dysregulation occurs depending on CAG repeat length and age, we conducted microarray-based expression profile analysis of the cerebrum and cerebellum of the Q76, Q113, Q129, and nTg mice at 4, 8, and 12 weeks of age. To determine the number of significantly dysregulated genes in the cerebrum or cerebellum of the transgenic mice compared with that of the nTg mice, we calculated the ratios of the intensities of individual probe sets of the Q76, Q113, and Q129 transgenic mice ($n = 3$) to those of the nTg mice ($n = 3$), and the p -values of each probe set from each single-colored Affymetrix MOE430 array intensity data set using the Ratio Builder and error model in the Rosetta Resolver System. Significantly dysregulated genes were selected on the basis of the cutoff p -value (≤ 0.01). The numbers of downregulated/upregulated genes in the cerebrum of Q76 (4, 8, and 12 weeks), Q113 (4, 8, and 12 weeks), and Q129 (4, 8, and 12 weeks) mice were (37/23, 147/190, and 100/51), (254/67, 396/361, and 419/157), and (676/613, 703/661, and 920/432), respectively (Figs. 2A, B). The numbers of downregulated/upregulated genes in the cerebellum of Q76 (4, 8, and 12 weeks), Q113 (4, 8, and 12 weeks), and Q129 (4, 8, and 12 weeks) mice were (81/46, 517/261, and 80/63), (179/63, 421/295, and 400/249), and (945/542, 782/560, and 834/532), respectively (Figs. 2C, D).

Agilent platform

For the two-colored data from the Agilent G4121A arrays, the intensity ratios were directly calculated on the basis of the obtained intensities of Cy3 and Cy5, which labeled respective cRNAs derived from the transgenic and nTg mice. For the analyses of three pairs of RNAs from

three transgenic samples (target) and three nTg samples (reference), six arrays (biological triplicate and dye swapping duplicate) were used for generating one final intensity ratio. Significantly dysregulated genes were selected on the basis of the cutoff p -value (≤ 0.01). The numbers of downregulated/upregulated genes in the cerebrum of Q76 (4, 8, and 12 weeks), Q113 (4, 8, and 12 weeks), and Q129 (4, 8, and 12 weeks) mice were (241/199, 304/340, and 422/312), (916/518, 1431/1367, and 1676/1452), and (2618/1912, 2188/2310, and 2660/2644), respectively (Figs. 2A, B). The numbers of downregulated/upregulated genes in the cerebellum of Q76 (4, 8, and 12 weeks), Q113 (4, 8, and 12 weeks), and Q129 (4, 8, and 12 weeks) mice were (167/171, 1360/1288, and 938/673), (571/707, 1562/1475, and 1885/1278), and (2759/2377, 2247/2112, and 2620/2187), respectively (Figs. 2C, D). In both the Affymetrix and Agilent platforms, the number of dysregulated genes tended to increase in a CAG-repeat-length-dependent manner as well as an age-dependent manner.

Cross-platform analysis

To obtain a confirmatory interpretation, we conducted a comprehensive cross-platform analysis using the Affymetrix and Agilent platforms. To evaluate the validity of cross-platform analysis, correlation coefficients and the number of commonly upregulated/downregulated genes were calculated from the intensity ratio data of each probe or probe set (on the basis of the Entrez gene) on both platforms. Correlation analysis demonstrated a high degree of correlation between the two platforms, and the number of correlated genes was far larger than that of anticorrelated genes. For example, in the Q129 mice at 4, 8, and 12 weeks of age, the correlation coefficients of common signature genes in both platforms were 0.83, 0.79, and 0.79, and the numbers of correlated/anticorrelated genes were 814/11, 695/21, and 901/11 (Supplementary Fig. 3), respectively, thus strongly confirming the validity of the cross-platform analysis.

Figs. 2A–D show a summary of the numbers of significantly dysregulated genes in the cerebrum and cerebellum of the transgenic mice determined by Affymetrix platform, Agilent platform, and cross-platform analyses. The significance of dysregulation was determined at a p -value of ≤ 0.01 for both platforms, which was calculated using the error model in the Rosetta Resolver System. The results showed that the numbers of downregulated/upregulated genes in the cerebrum of Q76 (4, 8, and 12 weeks), Q113 (4, 8, and 12 weeks), and Q129 (4, 8, and 12 weeks) mice were (2/0, 7/9, and 22/8), (121/13, 215/94, and 297/79), and (466/348, 448/247, and 643/267), respectively, and that the numbers of downregulated/upregulated genes in the cerebellum of Q76 (4, 8, and 12 weeks), Q113 (4, 8, and 12 weeks), and Q129 (4, 8, and 12 weeks) were (4/8, 97/44, and 41/22), (41/12, 177/103, and 283/141), and (599/351, 444/265, and 558/345), respectively (shown by red bars in Figs. 2A–D). The number of significantly dysregulated genes in both the cerebrum and cerebellum tended to increase with CAG repeat length. In the Q76 mice, which showed only mild phenotypic changes, the number of significantly dysregulated genes was very small throughout the period of observation. However, in the Q113 and Q129 mice, which exhibited severely impaired motor coordination, the number of significantly dysregulated genes was markedly larger. Cross-platform analysis also revealed that the number of downregulated genes was much larger than that of upregulated genes. These findings suggest that the CAG-repeat-length-dependent alteration, especially the downregulation, of gene expression may have a contextual connection with the development of motor phenotypes in the DRPLA transgenic mice.

Two-dimensional cluster analysis and gene annotation enrichment analysis revealed functional groups of genes showing CAG repeat length- and age-dependent changes in expression levels

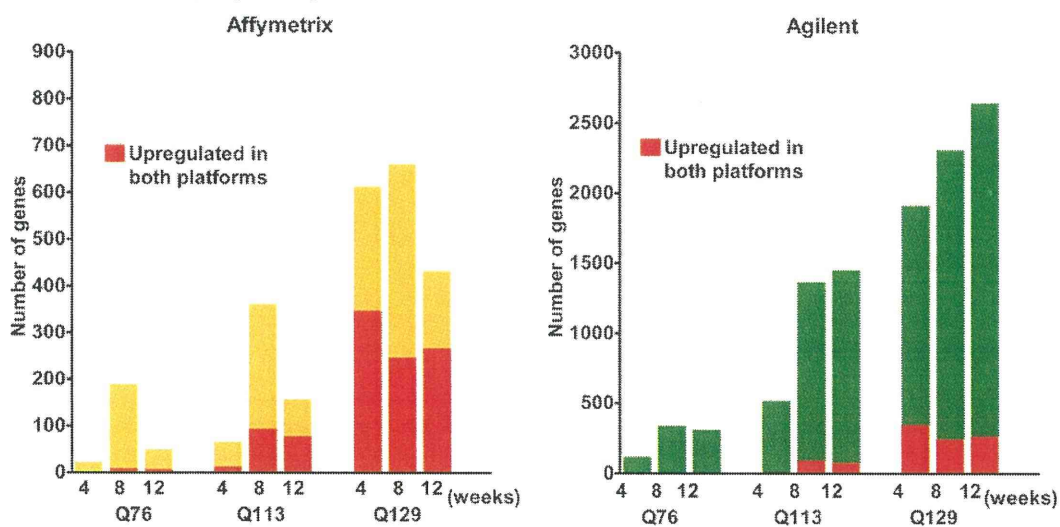
Besides the number of genes, the biological functions of the genes whose expression levels changed depending on the CAG repeat length

and age are expected to be relevant to the effects of the size of expanded CAG repeats and age on the pathogenetic process of the disease. To determine the categories of the genes that showed CAG-repeat-length- and age-dependent changes in expression level, we performed a series of analyses, namely, ANOVA, agglomerative cluster analysis, and gene annotation analysis. The gene identification algorithm and outline are shown in Fig. 3. The genes whose expression levels changed depending on the CAG repeat length and age were selected at interaction p-values of less than 0.005 by two-way [strain (Q76, Q113, Q129, nTg) and age (4, 8, 12 weeks)] ANOVA. According to this criterion, 879, 1412, and 204 genes in the cerebrum were identified to show expression level changes depending on the CAG repeat length and age by Affymetrix platform, Agilent platform, and cross-platform analyses, respectively. Similarly, 1037, 2943, and 431 genes in the cerebellum were identified by these analyses. Cluster analysis was performed for the genes found to be commonly altered by the cross-platform analysis using the

agglomerative clustering algorithm in the Rosetta Resolver system. Results are shown as an intensity (converted into Z-score) matrix using the data obtained by Affymetrix platform analysis.

Fig. 4A shows the results of the cluster analysis of the 204 genes that were found to be significantly altered in the cerebrum by both the Affymetrix and Agilent platform analyses. The genes were categorized into three clusters. The 102 genes belonging to cluster 1 tended to be downregulated with increasing CAG repeat length and age. In contrast to cluster 1, the numbers of altered genes in clusters 2 and 3 were limited. The 45 genes belonging to cluster 2 tended to be upregulated with increasing CAG repeat length and age. The 53 genes belonging to cluster 3 were markedly upregulated in the Q129 mice, which showed the severest phenotype from a very early stage (4 weeks) of the disease. These genes also tended to be upregulated in transgenic strains of Q113 mice. The genes included in each cluster are shown in Supplementary Table 1A.

A. Cerebrum: Upregulate genes



B. Cerebrum: Downregulate genes

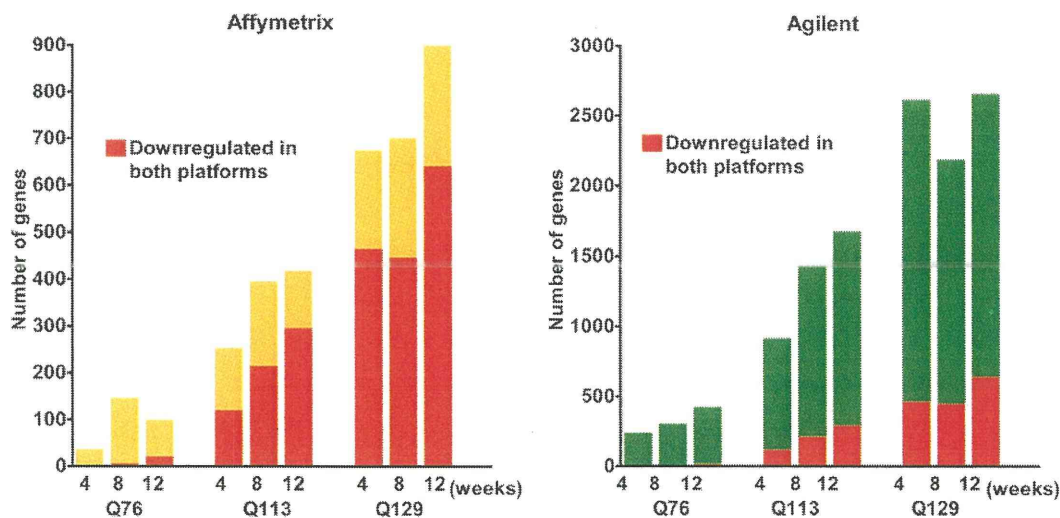
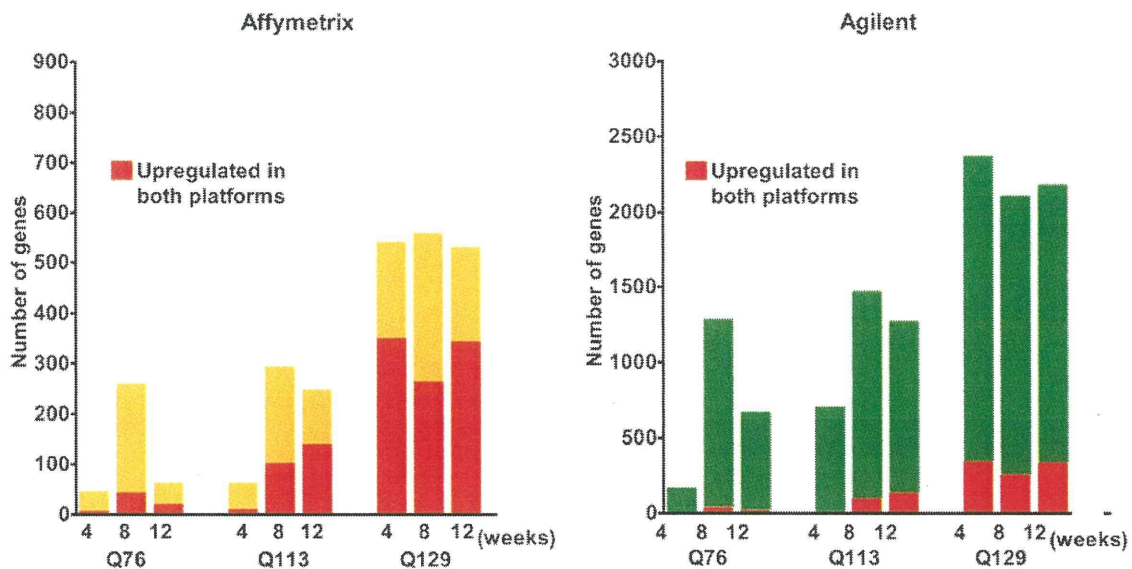


Fig. 2. Number of altered genes in the brains of DRPLA transgenic mice across platforms. The data shown in A–D are the numbers of upregulated or downregulated genes identified by Affymetrix platform (MOE430A) and Agilent platform (mouse 22K oligo array G4121A) analyses in either the cerebrum or the cerebellum of the Q76, Q113, and Q129 mice using a cutoff p-value of ≤ 0.01 , compared with the nTg control. The numbers of genes identified by cross-platform analyses are shown in red columns. The error model of Rosetta Resolver is used for analysis of raw data obtained by both Affymetrix and Agilent platform analyses. A. Upregulated genes in the cerebrum of DRPLA transgenic mice. B. Downregulated genes in the cerebrum of DRPLA transgenic mice. C. Upregulated genes in the cerebellum of DRPLA transgenic mice. D. Downregulated genes in the cerebellum of DRPLA transgenic mice.

C. Cerebellum: Upregulated genes



D. Cerebellum: Downregulated genes

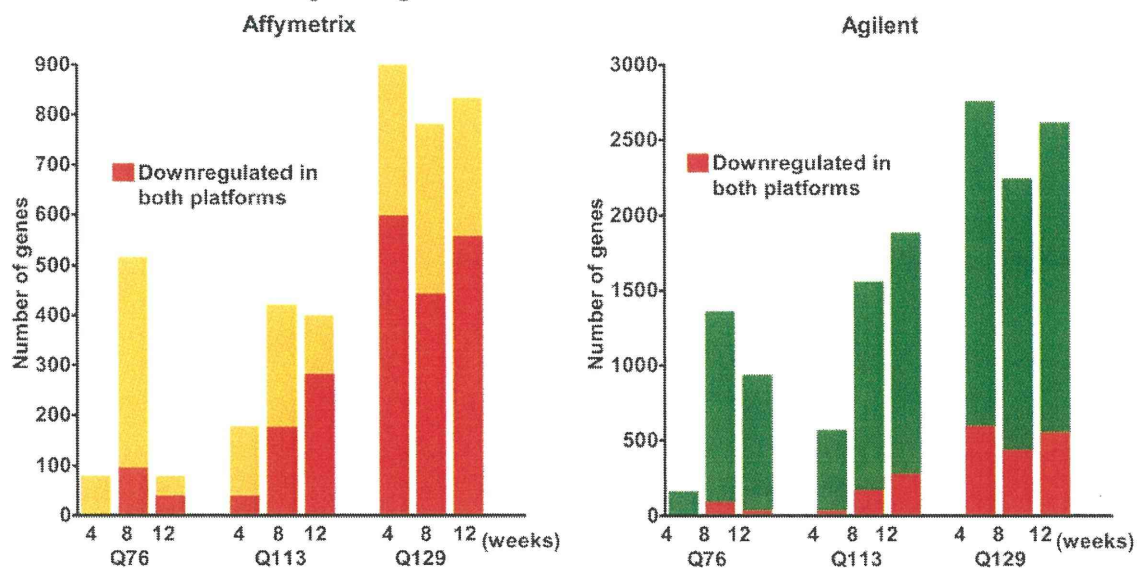


Fig. 2 (continued).

To identify relevant biological pathways associated with each cluster, gene–gene ontology (GO) term and gene–Kyoto Encyclopedia of Genes and Genomes (KEGG) pathway enrichment analysis was performed on the basis of an EASE score (p -value ≤ 0.05) calculated using DAVID (<http://david.abcc.ncifcrf.gov/>). The GO terms in the biological process and molecular function categories of the genes significantly enriched in each cluster are shown in Table A. (Complete data are shown in Supplementary Table 2A).

The expression levels of the genes in cluster 1 gradually decreased with increasing CAG repeat length and age. Gene annotation enrichment analysis demonstrated that the ion-transportation-related GO terms, particularly calcium ion transport for the category of the biological process, were highly enriched in this gene cluster. In addition, cell–cell-adhesion-related and signal-transduction-related terms (neuropeptide signaling pathway and intracellular signaling cascade) were also enriched. In the molecular function category, the terms related to protein binding functions topped the list, and calmodulin binding, in

particular, was conspicuous ($p = 1.15 \times 10^{-5}$). Cytoskeleton protein (including actin) binding was also highly rated. In this context, pathway enrichment analysis revealed that three KEGG pathways were enriched in this cluster, namely, the calcium signaling pathway and its two downstream pathways: the phosphatidylinositol signaling pathway and the MAPK signaling pathway (Supplementary Table 2A).

By contrast, cluster 2 was highly enriched with the GO terms of cellular metabolism, particularly protein modification. This finding was supported by another finding that protein-kinase-activity-related terms were highly rated in the molecular function category. Among others, nucleotide binding, especially RNA binding, topped the list. Cluster 3 was uniquely characterized by being enriched with the terms related to cell death and apoptosis, and the regulation of these processes. This tendency probably reflects the early changes in gene expression arising from the neuronal degeneration process and biological responses to the strong disease insult in transgenic strains with largely expanded CAG repeats.

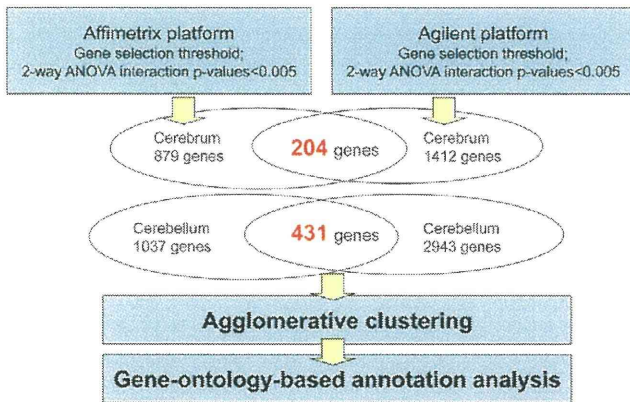


Fig. 3. Gene identification across platforms and strategy for cross-platform analysis. The genes whose expression levels changed depending on the CAG repeat length and age were selected at an interaction p-value of ≤ 0.005 by 2-way [strain (Q76, Q113, Q129, and nTg) and age (4, 8, and 12 weeks)] ANOVA. According to this criterion, 879, 1412, and 204 genes in the cerebrum were identified to show expression level changes depending on CAG repeat length and age in Affymetrix, Agilent, and cross-platform analyses, respectively. Similarly, 1037, 2943, and 431 genes in the cerebellum were identified. Cluster analysis was performed on the genes found to be commonly altered in the cross-platform analysis using the agglomerative clustering algorithm in the Rosetta Resolver system. The gene ontology terms and biological pathways related to each cluster are identified using gene-ontology-based annotation analysis.

Fig. 4B shows the result of the cluster analysis of the 431 genes that were found to be significantly altered in the cerebellum by both Affymetrix and Agilent platform analyses. Intriguingly, these genes that were altered in the cerebellum were also classified into three clusters, which showed marked similarity to those in the cerebrum with regard to the trend and pattern of expression. The genes included in each cluster are shown in Supplementary Table 1B. The numbers of genes included in clusters 1, 2, and 3 were 153, 167, and 111, respectively. These three clusters in the cerebellum shared considerable numbers of genes with the corresponding clusters in the cerebrum. Indeed, 30, 26, and 30 genes in the clusters 1, 2, and 3 in the cerebellum were also included in the clusters 1, 2, and 3 in the cerebrum, respectively (Supplementary Fig. 4). Genes commonly included in the corresponding clusters are indicated by an asterisk in Supplementary Tables 1A and 1B. The results of annotation analysis are shown in Table B (Complete data are shown in Supplementary Table 2B). In contrast to the same cluster in the cerebrum, cluster 1 in the cerebellum was clearly characterized by the overrepresentation of neuron-developmental-process-related terms, although a similar enrichment of the intracellular-signaling-cascade-related terms was also observed in this cluster in the cerebellum. In the molecular function category, the overrepresentation of terms related to ion binding/calcium ion binding was also observed in this cluster in the cerebellum as observed in the cerebrum. The genes in cluster 2, which were upregulated with increasing CAG repeat length and age, were mainly associated with protein metabolism/kinase activity and nucleic acid binding, most of which are common to those in the same cluster in the cerebrum both in the biological process and molecular function categories. Among the genes in cluster 3 in the cerebellum, which were also upregulated exclusively in the Q129 strain, cellular-metabolism-related terms were highly rated. Moreover, the terms related to transcription (e.g., transcription and regulation of transcription, DNA-dependent) and their related processes including the epigenetic regulation system (e.g., RNA splicing, DNA packaging, and chromatin assembly or disassembly) were uniquely enriched in this gene cluster. The genes related to cell death/apoptosis were also included and highly rated in cluster 3 in the cerebellum (30 genes were commonly included in cluster 3 in both the cerebrum and cerebellum), but the occupancy of these genes was lower than that in the cerebrum.

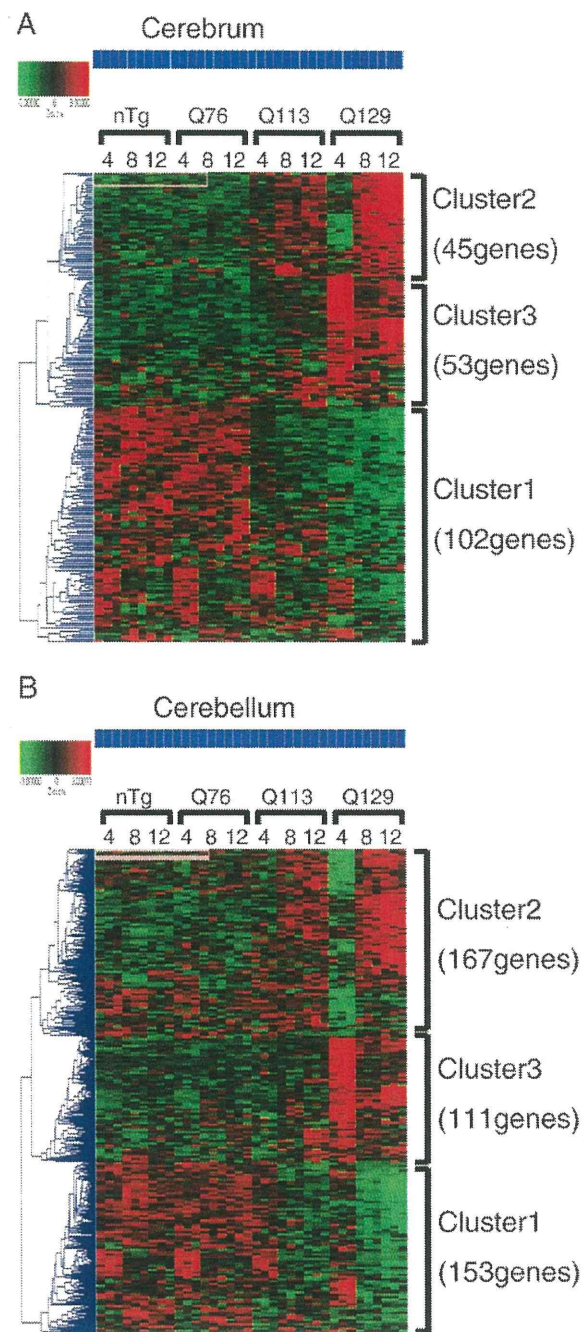


Fig. 4. Agglomerative cluster analysis of genes found to be significantly altered in both Affymetrix and Agilent platform analyses. A. Cluster analysis of the 204 altered genes in the cerebrum of DRPLA transgenic mice. B. Cluster analysis of the 431 altered genes in the cerebellum of DRPLA transgenic mice. The results are shown as an intensity (converted into Z-score) matrix using the data obtained by Affymetrix platform analysis. Each column represents a single sample at a certain time point for a certain mouse strain and each time point has three replicates. Each row represents a single gene, and the gene clusters are shown by the hierarchical cluster trees to the left of the columns. Red represents a higher Z-score (higher expression level) and green represents a lower Z-score (lower expression level).

As shown in Fig. 4, the expression profiles in the three clusters of Q76 in cerebrum (Fig. 4A) and cerebellum (Fig. 4B) look similar to those of nTg mice, while those of Q113 and Q129 show similar patterns. These observations raise a fundamental question, “Is there a

significant overlap in the genes changing (trends), or are there fundamentally different transcripts changing in between the mice with the larger expansions (Q113 and Q129) and those with the smaller expansion (Q76)?" To address this question, we further investigated the relationships of significantly dysregulated genes in the Q76, Q113 and Q129 mice at the age of 12 weeks determined by cross-platform analysis (correspond to the red bars in Figs. 2A–D). Interestingly, over half of downregulated genes in the Q76 mice were also downregulated both in the Q113 and Q129 mice (Supplementary Fig. 5), suggesting that downregulated genes were essentially similar across three transgenic strains although the numbers of them were drastically increased depending on the size of expanded CAG repeats. On the other hand, there was no overlap in the upregulated genes in the cerebrum of the Q76 mice with those of the Q113 and Q129 mice. In the cerebellum of the Q76 mice, only a limited portion of the upregulated genes overlapped with those of the Q113 mice and Q129 mice. These observations suggest that the upregulated genes are relatively specific to the Q113 and Q129 mice, which can be regarded as the specific response to the very largely expanded polyglutamine stretches.

Discussion

DRPLA transgenic mouse lines harboring variable lengths of expanded CAG repeats exhibit CAG repeat length- and age-dependent phenotypic changes resembling those in human DRPLA

CAG-repeat-length-dependent phenotypic variation is a cardinal feature commonly observed in polyglutamine diseases including DRPLA. To accurately evaluate the CAG-repeat-length-dependent phenotypic variations in transgenic mice, various parameters including the promoter, the context, the insertion site, and the copy number of the transgene need to be identical. To accomplish this, we have generated DRPLA transgenic mouse strains carrying various lengths of CAG repeats (Q76, Q96, Q113, and Q129) on a homogeneous genetic background. The transgenic mouse strain with the longest CAG repeat expansion (Q129) exhibits very severe and progressive phenotypes closely resembling those of early-onset human DRPLA, such as ataxia, epilepsy, and myoclonus, whereas the transgenic strain with the shortest CAG repeat expansion (Q76) shows no obvious DRPLA phenotype (Sato et al., 2009). The mouse lines with moderately expanded CAG repeats (Q96 and Q113) showed intermediate phenotypes depending on the CAG repeat length (Fig. 1). Thus, we have successfully reproduced the CAG-repeat-length-dependent phenotypic features of DRPLA in the transgenic models we generated in this study. This study is the first *in vivo* demonstration of the CAG repeat length and age dependence of mouse phenotypes and gene expression changes in polyglutamine diseases.

The transgenic strains with expanded CAG repeats of 96 and above showed obvious motor deficits, whereas the strain with 76 CAG repeats (Q76) did not seem to show any decline in motor performance (Fig. 1), despite the existence of region-specific accumulation of the mutant DRPLA protein in the brain (Sato et al., 2009). Seventy-six CAG repeats are sufficiently long to induce the development of the disease phenotypes of DRPLA in humans. The number of CAG repeats in DRPLA patients is generally increased to over 50, whereas that in normal individuals is usually under 30. The lifespans are tremendously different between humans and mice. As we have indicated, the accumulation of the mutant proteins is not only a CAG-repeat-length-dependent but also a time-dependent process. In the case of our Q76 transgenic strain, the lifespan of the mice is probably too short to develop motor deficits resulting from progressive intranuclear accumulation of mutant DRPLA proteins, which take years or decades to show up in DRPLA patients.

In this study, we demonstrated that transgenic mice with relatively short CAG repeats (Q76 and Q96) show deficits in spatial learning and memory in the early stage of the disease. Previous studies on other

mouse DRPLA models did not pay much attention to memory disturbance, while motor phenotypes were mainly highlighted. This study is the first to show cognitive impairment of DRPLA transgenic mice. Cognitive impairment and character changes are, in fact, major symptoms in DRPLA patients. Besides DRPLA, cognitive impairment is the common clinical presentation of polyglutamine diseases, particularly Huntington's disease. In previous studies, cognitive impairment was reproduced in transgenic mice with Huntington's disease (Lione et al., 1999; Van Raamsdonk et al., 2005). Since our series of DRPLA transgenic mice clearly showed CAG-repeat-length-dependent deterioration of DRPLA phenotypes, we were able to easily observe the cognitive impairment (Q76 and Q96) before these phenotypes were masked by motor impairment.

Cross-platform analyses confirmed CAG-repeat-length- and age-dependent changes in expression profiles

Microarray-based expression profiling is widely used to search for the genes related to disease pathogenesis. In general, the genes identified as "significantly dysregulated" need to be confirmed by independent experiments, usually by real-time RT-PCR or northern blot analyses. However, it is impractical to confirm a large number of genes by those approaches. To overcome this limitation, we performed a comprehensive cross-platform analysis using two different microarray platforms, which employ completely different probe designs and algorithms, to confirm the significantly dysregulated genes identified by single-platform analysis. The combined use of Affymetrix arrays and Agilent arrays has shown that there is a high correlation between these two platforms, and the number of correlated genes is by far larger than that of anticorrelated genes, strongly supporting the validity of the cross-platform analysis for the high-throughput confirmation of microarray data.

As shown in Fig. 4, two-dimensional cluster analyses of the cross-platform data revealed three clusters. In cluster 1, genes were downregulated with increasing CAG repeat length and age. In contrast to cluster 1, genes were upregulated with increasing CAG repeat length and age in cluster 2. In cluster 3, genes were exclusively upregulated in the Q129 mice at an early stage. These findings further confirm that the length of expanded CAG repeats and age, which are the major determinants of neuronal intranuclear accumulation of mutant DRPLA proteins, also play a critical role in the severity of transcriptional dysregulation.

Although the changes in the expression profiles are very mild in Q76 (Fig. 4), a substantial number of downregulated genes in the Q76 mice were also downregulated in the Q113 and Q129 mice, confirming that mice with smaller expansions show essentially the same trends as with larger ones in terms of downregulation of genes (Supplementary Fig. 5). In contrast, there was no overlap in the upregulated genes in the cerebrum of Q76 mice with those of the Q113 or Q129 mice. In the cerebellum of the Q76 mice, only a limited portion of the upregulated genes overlapped with those of Q113 mice or Q129 mice. Thus, upregulation of genes is rather specific to the Q113 and Q129 mice, presumably reflecting the cellular response to the very largely expanded polyglutamine stretches.

Downregulated genes are associated with calcium signaling, neuropeptide signaling, and neuronal development

The overrepresentation of gene annotation terms related to calcium signaling and calcium binding proteins was observed to be the prominent feature of the genes in cluster 1 (Table A). Previous microarray studies have mainly indicated that neurotransmitters and their receptors are downregulated in animal models of polyglutamine diseases (Luthi-Carter et al., 2000, 2002), but none of them have identified the specifically dysregulated genes related to calcium signaling pathways. In this study, we have specifically identified the downregulated genes

related to calcium signaling (e.g., *Plcb1*, *Ppp3Ca*, *Pde1b*, *Itpka*, *Itp1*, and *Atp2b2*) and calmodulin binding, which, consistent with recent findings indicating the possible involvement of calcium signaling in the pathogenesis of Huntington's disease (Panov et al., 2002; Tang et al., 2003, 2005; Varshney and Ehrlich, 2003), may represent dysfunction in calcium signaling and contribute to the molecular mechanism of neuronal dysfunction in DRPLA.

Specifically, the downregulation of inositol 1,4,5-triphosphate receptor 1 (*Itp1*) deserves special attention. The expression level of *Itp1* has been demonstrated to be decreased in mouse models of Huntington's disease (Luthi-Carter et al., 2000) and SCA1 (Lin et al., 2000). The *Itp1*-encoded protein forms a complex with Huntingtin, which affects calcium signaling (Tang et al., 2003), and *Itp1* KO mice show ataxia and epileptic seizures (Matsumoto et al., 1996). Large deletions involving *Itp1* have recently been identified in patients with SCA15 (Hara et al., 2008; van de Leemput et al., 2007). Thus, the downregulation of *Itp1* identified in this study further indicates that the dysfunction of calcium signaling caused by the downregulation of calcium-signaling-related genes including *Itp1* is potentially involved in the pathogenesis of polyglutamine diseases including DRPLA.

Previously, we reported the downregulation of hypothalamic neuropeptide genes in Q129 mice (Sato et al., 2009). Confirming this finding, our present study also demonstrated the CAG repeat length- and age-dependent downregulation of hypothalamic neuropeptide genes in the cerebrum of DRPLA transgenic mice, such as *Penk1*, *Npy*, *Cart*, and *Sst*. The downregulation of these hypothalamic neuropeptide genes may contribute to the phenotypic manifestations potentially caused by the dysfunction of the hypothalamus that we have observed in the DRPLA transgenic mice, such as progressive body weight loss and central diabetes insipidus (Sato et al., 2009). The downregulation of hypothalamic neuropeptide genes and hypothalamic dysfunction have also been observed in a mouse model of Huntington's disease (Kotliarova et al., 2005). Previous studies have demonstrated the decreased expression levels of hypothalamic neuropeptides [i.e., proenkephalin (Iadarola and Mouradian, 1989) and somatostatin (Cramer et al., 1981)] in the cerebrospinal fluid of patients with Huntington's disease. It is possible that the downregulation of hypothalamic neuropeptide genes causes subclinical endocrinological dysfunctions, which then may contribute to mood changes or psychotic symptoms in DRPLA patients.

Table

Function categories of the gene clusters. A. Function categories of the gene clusters in the cerebrum. B. Function categories of the gene clusters in the cerebellum. The table shows the gene ontology (GO) terms of the genes significantly enriched in each cluster in either the cerebrum or cerebellum of the DRPLA transgenic mice and their biological process and molecular function categories. The GO terms were selected on the basis of a p -value ≤ 0.05 , which is calculated using EASE. Other similar significant terms, cellular component category terms, and KEGG pathways are not included to minimize redundancy. Terms are considered "similar" if two terms have the same the parent term or both the parent and child (or grandchild) terms are included together. Complete data are shown in the Supplementary Table 2A, B.









A. Cerebrum			
Biological process	p value	Molecular function	p value
Cluster 1			
Metal ion transport	0.00549	Calmodulin binding	0.00001
Calcium ion transport	0.01266	Protein binding	0.00014
Cell-cell adhesion	0.01499	Binding	0.00461
Neuropeptide signaling pathway	0.01520	Actin binding	0.00522
Intracellular signaling cascade	0.01607	Calcium ion binding	0.00700
Cation transport	0.02138	Ion binding	0.01175
Negative regulation of biological process	0.02405	Metal ion binding	0.01175
Neurotransmitter transport	0.02608	Cation binding	0.01796
Negative regulation of cellular process	0.03944	Cytoskeletal protein binding	0.02326
Di-, tri-valent inorganic cation transport	0.03974	Cation transporter activity	0.02351
 Ion transport		 Protein binding	
 Cell signaling		 Ion binding	
Cluster 2			
Cellular metabolism	0.00488	RNA binding	0.00057
Cell division	0.00967	Nucleotide binding	0.00138
Biopolymer metabolism	0.01282	Nucleic acid binding	0.00470
Protein modification	0.02550	Binding	0.01242
Cellular protein metabolism	0.02965	Protein serine/threonine kinase activit	0.02170
Biopolymer modification	0.03112	Enzyme regulator activity	0.04203
Cellular macromolecule metabolism	0.03273	Protein kinase activity	0.04395
Embryonic development	0.03417	Cyclin-dependent protein kinase regulator activi	0.04617
Phosphate metabolism	0.04921		
Phosphorus metabolism	0.04921		
 Protein modification		 Nucleotide/nucleic acid binding	
 Protein kinase			
Cluster 3			
Positive regulation of cellular process	0.00321	Copper ion binding	0.00862
Negative regulation of apoptosis	0.00348	Binding	0.01624
Negative regulation of programmed cell death	0.00365	Insulin-like growth fa	0.04298
Regulation of cell proliferation	0.00369	Integrin binding	0.04498
Negative regulation of cellular process	0.00745		
Apoptosis	0.00902		
Fatty acid biosynthesis	0.00920		
Cell-substrate adhesion	0.00952		
Regulation of apoptosis	0.00975		
Programmed cell death	0.00978		
 Cell death/apoptosis			

Table (continued)

B. Cerebellum			
Biological process	p value	Molecularfunction	p value
Cluster 1			
Cell development	0.0000	Protein binding	0.0000
Neuron differentiation	0.0001	Calcium ion binding	0.0001
Neuron development	0.0001	Receptor binding	0.0005
Positive regulation of locomotion	0.0001	Cation binding	0.0009
Positive regulation of cell motility	0.0001	GTPase regulator activity	0.0010
Cell differentiation	0.0002	Ion binding	0.0019
Neurogenesis	0.0003	Metalion binding	0.0019
Development	0.0004	Binding	0.0020
Intracellular signaling cascade	0.0004	Enzyme regulator activity	0.0060
Nervous system development	0.0006	Lipid binding	0.0070
Cell migration/differentiation/development		Ion binding	
Cluster 2			
Cellular physiological process	0.0000	Protein binding	0.0000
Negative regulation of biological process	0.0000	Nucleotide binding	0.0000
Protein processing	0.0000	Purine nucleotide binding	0.0002
Protein metabolism	0.0000	RNA binding	0.0004
Primary metabolism	0.0001	ATP binding	0.0005
Biopolymer modification	0.0003	Protein dimerization activity	0.0011
Metabolism	0.0003	Transferase activity, transferring phosphorus-	0.0016
Macromolecule metabolism	0.0004	Protein serine/threonine kinase activity	0.0018
Cellular protein metabolism	0.0005	Kinase activity	0.0043
Cell organization and biogenesis	0.0005	cAMP-dependent protein kinase activity	0.0052
Protein modification		Nucleotide/nucleic acid binding	
		Protein kinase	
Cluster 3			
Biopolymer metabolism	0.0002	Obsolete molecular function	0.0001
Cellular physiological process	0.0005	Binding	0.3100
RNA splicing, via transesterification reactions	0.7000	Nucleic acid binding	0.1800
RNA splicing	0.0008	RNA binding	0.0319
DNA packaging	0.0011	Protein binding	0.0331
DNA metabolism	0.0014	Chondroitin sulfate proteoglycan	0.0335
Regulation of cell proliferation	0.7100	Nucleotide binding	0.8330
mRNA processing	0.0025	Copper ion binding	0.0420
Regulation of transcription, DNA-dependent	0.0029		
Transcription	0.0034		
RNA splicing		Regulation of transcription	
		Nucleotide/nucleic acid binding	

The genes downregulated in the cerebellum (cluster 1) are found to be mostly related to neuronal developmental processes. In particular, the downregulation of the genes related to myelination (e.g., *Cldn11*, *Ugr8a*, *Plp1*, and *Large*) are noteworthy, since these genes may play a role in the formation of white matter lesions, which are characteristically observed in DRPLA patients. Our previous morphometric study has also demonstrated that spine density is reduced in the neurons of Q129 DRPLA mice (Sakai et al., 2006). Neuropathological observations have long revealed that the entire brain of DRPLA patients is somehow proportionally small in addition to the region-specific neuronal loss in the dentatorubral and pallidolusian systems. Considering these findings, developmental abnormalities of neurons are also considered as important pathological processes in DRPLA, besides neuronal degeneration.

We previously demonstrated the age-dependent downregulation of genes in the cerebrum of Q129 DRPLA transgenic mice (Sato et al., 2009). Among the 46 genes from that study, 10 genes were also identified to be associated with age-dependent as well as CAG-repeat-length-dependent downregulation in our present study (included in cluster 1). Four of the 10 genes encode transcription factors (*Dbp*, *Egr1*, *Bhlhb2*, and *Mef2c*), three encode neuropeptides (*Sst*, *Npy*, and *Penk1*), one encodes a signaling molecule (*Prkcd*), one encodes a vesicular transporter (*Rab33a*), and one encodes a cytoskeletal and structural molecule (*Cldn11*). Six of the 21 genes listed as CREB-dependent genes are

included in cluster 1 (*Sst*, *Penk1*, *Egr1*, *Bhlhb2*, *Mef2c*, and *Cldn11*). Intriguingly, the genes found to be downregulated in both our present and previous studies are functionally categorized into the same categories: neuropeptide genes, transcription factor genes, or CREB target genes. We previously demonstrated that CREB-dependent transcriptional activation is strongly suppressed by expanded polyQ stretches in cellular models (Nucifora et al., 2001; Shimohata et al., 2000, 2005), which strongly indicates that expanded-polyQ-mediated transcriptional suppression is involved in the pathogenesis of DRPLA. Our findings further support recent studies that demonstrated the therapeutic effectiveness of potent transcriptional activators, such as sodium butyrate (Ferrante et al., 2003; Ying et al., 2006), SAHA (Hockly et al., 2003), and phenylbutyrate (Gardian et al., 2005), against polyglutamine diseases.

Upregulated genes are associated with protein modification, apoptosis, and transcriptional regulation

The upregulated genes in transgenic models of polyglutamine diseases have been paid less attention than the downregulated genes, since they were regarded as the result of cellular stress responses and inflammation (Luthi-Carter et al., 2000, 2002). In this study, however, we have identified a cluster of genes that are upregulated with increasing

CAG repeat length and age (cluster 2), which have important biological functions, such as those encoding nucleotide-binding proteins, kinases, and phosphatases. Furthermore, most of these genes encode the proteins localized in the nucleus where the DRPLA protein acts as a transcriptional coregulator. Therefore, it is likely that the upregulation of these genes indicates their involvement in the intrinsic molecular interactions underlying the neuronal degeneration in the disease (Shen et al., 2007), instead of being simply a response to stress or inflammation.

It is interesting that the genes classified into cluster 3 in both the cerebrum and cerebellum in this study, which are exclusively upregulated in the Q129 transgenic strain from a very early stage, are mainly related to cell death and apoptosis (*Cdkn1a*, *Sgk*, *Trp53inp1*, *Tsc22d3*, and *Agt*). The *Cdkn1a*-encoded protein inhibits cell cycle progression in G1 by binding to G1 cyclin-CDK complexes, and cell cycle arrest in the G(0)/G(1) phase has been shown to enhance the cellular toxicity of truncated ataxin-3 with expanded polyQ stretches, which is the product of *MJD1* – the causative gene for Machado–Joseph disease/SCA3 (Yoshizawa et al., 2000). Thus, the upregulation of *Cdkn1a* in the brain of the DRPLA transgenic mice may indicate a similar role of the gene in enhancing the neuronal toxicity of the mutant DRPLA protein with expanded polyglutamine stretches. The upregulation of genes whose function is neuroprotective (negative regulation of apoptosis or programmed cell death), such as *Sgk*, may indicate a protective response to the neuronal toxicity of the mutant DRPLA protein containing expanded polyQ stretches. Interestingly, the expression level of *Sgk* has also been reported to be elevated in the brain of patients with Huntington's disease (Rangone et al., 2004).

Conclusions

We have unprecedentedly generated DRPLA transgenic mouse strains carrying various lengths of expanded CAG repeats, and demonstrated significant CAG repeat length- and age-dependent changes in behavioral phenotypes and gene expression profiles in the transgenic mice. We have identified specific gene clusters that are differentially dysregulated in the brains of the animals and new pathways that are potentially involved in the pathogenesis of DRPLA. This study is the first to comprehensively reproduce the CAG repeat length- and age-dependent features of human DRPLA in animal models, and has provided new insights into the pathogenic mechanisms leading to neuronal degeneration and dysfunction in DRPLA as well as in other polyglutamine diseases.

Funding

This work was supported in part by KAKENHI (Grant-in-Aid for Scientific Research) on Priority Areas (Applied Genomics, Advanced Brain Science Project, and Integrative Brain Research), the 21st Century COE Program, Center for Integrated Brain Medical Science and Scientific Research (A) from the Ministry of Education, Culture, Sports, Science and Technology, Japan, and a grant from the Research Committee for Ataxic Diseases, the Ministry of Health, Labour and Welfare, Japan.

Acknowledgments

We thank Ms. Mari Miyamoto (Rosetta Biosoftware), Dr. Rui Yamaguchi, Dr. Seiya Imoto, and Dr. Satoru Miyano (Laboratory of DNA Information Analysis, Human Genome Center, Institute of Medical Science, University of Tokyo) for their helpful discussions, and Ms. Chinami Kajiwara and Mrs. Masako Koizumi for management of laboratory animal facilities.

Appendix A. Supplementary data

Supplementary data to this article can be found online at doi:10.1016/j.nbd.2012.01.014.

References

- Carter, R.J., et al., 1999. Characterization of progressive motor deficits in mice transgenic for the human Huntington's disease mutation. *J. Neurosci.* 19, 3248–3257.
- Cramer, H., et al., 1981. Huntington's chorea – measurements of somatostatin, substance P and cyclic nucleotides in the cerebrospinal fluid. *J. Neurol.* 225, 183–187.
- David, G., et al., 1997. Cloning of the SCA7 gene reveals a highly unstable CAG repeat expansion. *Nat. Genet.* 17, 65–70.
- Dennis Jr., G., et al., 2003. DAVID: Database for Annotation, Visualization, and Integrated Discovery. *Genome Biol.* 4, P3.
- Erkner, A., et al., 2002. Grunge, related to human Atrophin-like proteins, has multiple functions in *Drosophila* development. *Development* 129, 1119–1129.
- Ferrante, R.J., et al., 2003. Histone deacetylase inhibition by sodium butyrate chemotherapy ameliorates the neurodegenerative phenotype in Huntington's disease mice. *J. Neurosci.* 23, 9418–9427.
- Gardian, G., et al., 2005. Neuroprotective effects of phenylbutyrate in the N171–82Q transgenic mouse model of Huntington's disease. *J. Biol. Chem.* 280, 556–563.
- Hara, K., et al., 2008. Total deletion and a missense mutation of ITPR1 in Japanese SCA15 families. *Neurology* 71, 547–551.
- Hockly, E., et al., 2003. Suberoylanilide hydroxamic acid, a histone deacetylase inhibitor, ameliorates motor deficits in a mouse model of Huntington's disease. *Proc. Natl. Acad. Sci. U. S. A.* 100, 2041–2046.
- Huang da, W., et al., 2009. Systematic and integrative analysis of large gene lists using DAVID bioinformatics resources. *Nat. Protoc.* 4, 44–57.
- Iadarola, M.J., Mouradian, M.M., 1989. Decrease in a proenkephalin peptide in cerebrospinal fluid in Huntington's disease and progressive supranuclear palsy. *Brain Res.* 479, 397–401.
- Ikeuchi, T., et al., 1995. Dentatorubral-pallidolysian atrophy (DRPLA): close correlation of CAG repeat expansions with the wide spectrum of clinical presentations and prominent anticipation. *Semin Cell Biol.* 6, 37–44.
- Imbert, G., et al., 1996. Cloning of the gene for spinocerebellar ataxia 2 reveals a locus with high sensitivity to expanded CAG/glutamine repeats. *Nat. Genet.* 14, 285–291.
- Kawaguchi, Y., et al., 1994. CAG expansions in a novel gene for Machado–Joseph disease at chromosome 14q32.1. *Nat. Genet.* 8, 221–228.
- Koide, R., et al., 1994. Unstable expansion of CAG repeat in hereditary dentatorubral-pallidolysian atrophy (DRPLA). *Nat. Genet.* 6, 9–13.
- Koide, R., et al., 1999. A neurological disease caused by an expanded CAG trinucleotide repeat in the TATA-binding protein gene: a new polyglutamine disease? *Hum. Mol. Genet.* 8, 2047–2053.
- Kotliarova, S., et al., 2005. Decreased expression of hypothalamic neuropeptides in Huntington disease transgenic mice with expanded polyglutamine-EGFP fluorescent aggregates. *J. Neurochem.* 93, 641–653.
- La Spada, A.R., et al., 1991. Androgen receptor gene mutations in X-linked spinal and bulbar muscular atrophy. *Nature* 352, 77–79.
- Lin, X., et al., 2000. Polyglutamine expansion down-regulates specific neuronal genes before pathologic changes in SCA1. *Nat. Neurosci.* 3, 157–163.
- Lindblad, K., et al., 1996. An expanded CAG repeat sequence in spinocerebellar ataxia type 7. *Genome Res.* 6, 965–971.
- Lione, L.A., et al., 1999. Selective discrimination learning impairments in mice expressing the human Huntington's disease mutation. *J. Neurosci.* 19, 10428–10437.
- Luthi-Carter, R., et al., 2000. Decreased expression of striatal signaling genes in a mouse model of Huntington's disease. *Hum. Mol. Genet.* 9, 1259–1271.
- Luthi-Carter, R., et al., 2002. Polyglutamine and transcription: gene expression changes shared by DRPLA and Huntington's disease mouse models reveal context-independent effects. *Hum. Mol. Genet.* 11, 1927–1937.
- Matsumoto, M., et al., 1996. Ataxia and epileptic seizures in mice lacking type 1 inositol 1,4,5-trisphosphate receptor. *Nature* 379, 168–171.
- Nagafuchi, S., et al., 1994. Dentatorubral and pallidolysian atrophy expansion of an unstable CAG trinucleotide on chromosome 12p. *Nat. Genet.* 6, 14–18.
- Naito, H., Oyanagi, S., 1982. Familial myoclonus epilepsy and choreoathetosis: hereditary dentatorubral-pallidolysian atrophy. *Neurology* 32, 798–807.
- Nakamura, K., et al., 2001. SCA17, a novel autosomal dominant cerebellar ataxia caused by an expanded polyglutamine in TATA-binding protein. *Hum. Mol. Genet.* 10, 1441–1448.
- Nucifora Jr., F.C., et al., 2001. Interference by huntingtin and atrophin-1 with cbp-mediated transcription leading to cellular toxicity. *Science* 291, 2423–2428.
- Orr, H.T., et al., 1993. Expansion of an unstable trinucleotide CAG repeat in spinocerebellar ataxia type 1. *Nat. Genet.* 4, 221–226.
- Panov, A.V., et al., 2002. Early mitochondrial calcium defects in Huntington's disease are a direct effect of polyglutamines. *Nat. Neurosci.* 5, 731–736.
- Pulst, S.M., et al., 1996. Moderate expansion of a normally biallelic trinucleotide repeat in spinocerebellar ataxia type 2. *Nat. Genet.* 14, 269–276.
- Rangone, H., et al., 2004. The serum- and glucocorticoid-induced kinase SGK inhibits mutant huntingtin-induced toxicity by phosphorylating serine 421 of huntingtin. *Eur. J. Neurosci.* 19, 273–279.
- Sakai, K., et al., 2006. Neuronal atrophy and synaptic alteration in a mouse model of dentatorubral-pallidolysian atrophy. *Brain* 129, 2353–2362.
- Sanpei, K., et al., 1996. Identification of the spinocerebellar ataxia type 2 gene using a direct identification of repeat expansion and cloning technique. *DIRECT. Nat. Genet.* 14, 277–284.
- Sato, T., et al., 2009. Severe neurological phenotypes of Q129 DRPLA transgenic mice serendipitously created by en masse expansion of CAG repeats in Q76 DRPLA mice. *Hum. Mol. Genet.* 18, 723–736.
- Sato, A., et al., 1999a. Adenovirus-mediated expression of mutant DRPLA proteins with expanded polyglutamine stretches in neuronally differentiated PC12 cells. Preferential intranuclear aggregate formation and apoptosis. *Hum. Mol. Genet.* 8, 997–1006.

- Sato, T., et al., 1999b. Transgenic mice harboring a full-length human mutant DRPLA gene exhibit age-dependent intergenerational and somatic instabilities of CAG repeats comparable with those in DRPLA patients. *Hum. Mol. Genet.* 8, 99–106.
- Shen, Y., et al., 2007. Functional architecture of atrophins. *J. Biol. Chem.* 282, 5037–5044.
- Shimohata, T., et al., 2000. Expanded polyglutamine stretches interact with TAFII130, interfering with CREB-dependent transcription. *Nat. Genet.* 26, 29–36.
- Shimohata, M., et al., 2005. Interference of CREB-dependent transcriptional activation by expanded polyglutamine stretches – augmentation of transcriptional activation as a potential therapeutic strategy for polyglutamine diseases. *J. Neurochem.* 93, 654–663.
- Tang, T.S., et al., 2003. Huntingtin and huntingtin-associated protein 1 influence neuronal calcium signaling mediated by inositol-(1,4,5) triphosphate receptor type 1. *Neuron* 39, 227–239.
- Tang, T.S., et al., 2005. Disturbed Ca^{2+} signaling and apoptosis of medium spiny neurons in Huntington's disease. *Proc. Natl. Acad. Sci. U. S. A.* 102, 2602–2607.
- The Huntington's Disease Collaborative Research Group, 1993. A novel gene containing a trinucleotide repeat that is expanded and unstable on Huntington's disease chromosomes. The Huntington's Disease Collaborative Research Group. *Cell* 72, 971–983.
- van de Leemput, J., et al., 2007. Deletion at ITPR1 underlies ataxia in mice and spinocerebellar ataxia 15 in humans. *PLoS Genet.* 3, e108.
- Van Raamsdonk, J.M., et al., 2005. Cognitive dysfunction precedes neuropathology and motor abnormalities in the YAC128 mouse model of Huntington's disease. *J. Neurosci.* 25, 4169–4180.
- Varshney, A., Ehrlich, B.E., 2003. Intracellular Ca^{2+} signaling and human disease: the hunt begins with Huntington's. *Neuron* 39, 195–197.
- Wood, J.D., et al., 2000. Atrophin-1, the dentato-rubral and pallido-luysian atrophy gene product, interacts with ETO/MTG8 in the nuclear matrix and represses transcription. *J. Cell Biol.* 150, 939–948.
- Yamada, M., et al., 2001. Widespread occurrence of intranuclear atrophin-1 accumulation in the central nervous system neurons of patients with dentatorubral-pallidoluysian atrophy. *Ann. Neurol.* 49, 14–23.
- Yamasaki, N., et al., 2008. Alpha-CaMKII deficiency causes immature dentate gyrus, a novel candidate endophenotype of psychiatric disorders. *Mol. Brain.* 1, 6.
- Ying, M., et al., 2006. Sodium butyrate ameliorates histone hypoacetylation and neurodegenerative phenotypes in a mouse model for DRPLA. *J. Biol. Chem.* 281, 12580–12586.
- Yoshizawa, T., et al., 2000. Cell cycle arrest enhances the in vitro cellular toxicity of the truncated Machado-Joseph disease gene product with an expanded polyglutamine stretch. *Hum. Mol. Genet.* 9, 69–78.
- Zhang, S., et al., 2002. Drosophila atrophin homolog functions as a transcriptional corepressor in multiple developmental processes. *Cell* 108, 45–56.
- Zhuchenko, O., et al., 1997. Autosomal dominant cerebellar ataxia (SCA6) associated with small polyglutamine expansions in the alpha 1A-voltage-dependent calcium channel. *Nat. Genet.* 15, 62–69.